Rational Regulation of Transition Metals in Polyoxometalate Hybrids without Noble-Metal Assistant for Efficient Light-Driven H_2 Production†

Bonan Li,[a†] Xiaojing Yu,[a†] Haijun Pang,[a*] Qingbo Shen,[a] Yan Hou,[a] Huiyuan Ma[a*] and Jianjiao Xin[a]

[a]School of Materials Science and Engineering, College of Chemical and Environmental Engineering, Harbin University of Science and Technology, Harbin, 150040, P. R. China

*E-mail: panghj116@163.com, Tel./fax.: 86-0451-86688575.

*E-mail: mahy017@163.com, Tel./fax: 86-0451-86392716.

Table of contents

Section 1 Experimental Section

I. Materials and General Methods

All other reagents were purchased commercially and were used without further purification. The FT-IR spectra were recorded from KBr pellets in the range of 4000–400 cm^{-1} with a Bruker OPTIK GmbH-Tensor II spectrometer. The powder X-ray diffraction (PXRD) data were collected on a Bruker OPTIK GmbH-Tensor II spectrometer at room temperature. Optical properties were also studied by diffuse reflectance UV-vis spectroscopy (Lambda 35 spectrometer), Photoluminescence spectrum (PL) (SPEX Fluorolog-3 spectrofluorometer). The X-ray photoelectron spectroscopy (XPS) measurements were implemented by a Thermo ESCALAB 250Xi spectrometer with monochromatic Al Kα radiation ($h\gamma$ = 1486.6 eV). All XPS spectra were characterized with respect to the C 1s peak at 284.8 eV.

The electrochemical impedance spectra (EIS), Mott-schottky plot and photocurrent-time (I-T) profiles was recorded on the CHI660E electrochemical workstation with a standard three-electrode system with the photocatalyst-coated ITO as the working electrode, Pt plate as the counter electrode, and Ag/AgCl electrode as a reference electrode. A 500 W Xenon lamp was used as the light source during the measurement. A 0.25 M Na_2SO_4 solution was used as the electrolyte. The as-synthesized samples (2 mg) were added into 1 mL ethanol and 10 μL Nafion mixed solution, and the working electrodes were prepared by dropping the suspension (200 μL) onto an ITO glass substrate electrode surface and dried at room temperature.

II. Synthesis of $Co^{II/III}_2$-SiW_{12}, $Fe^{II/III}_2$-SiW_{12}, Zn^{II}_2-SiW_{12} and Cd^{II}_2-SiW_{12}

The mixture of $H_4[SiW_{12}O_{40}]\cdot 12H_2O$ (320 mg, 0.096 mmol), $CoCl_2\cdot 6H_2O$ (160 mg, 0.672 mmol), pzta (40 mg, 0.272 mmol), and deionized water (12 mL) was intensively mixed for 90 min. Then, the mixture was loaded in a 23 mL hydrothermal reactor and heated at 160 °C for 72 h. The initial pH of the solution was 1.8 and adjusted to a final pH of 3.0 with 1M NaOH. After the autoclave was cooled to room temperature at 10 °C h^{-1}, Orange block crystals (Fig. S1) of **$Co^{II/III}_2$-SiW_{12}** were obtained (65% yield based on W). The reproducibility of **$Co^{II/III}_2$-SiW_{12}** is good. Elemental analysis calcd (%) for $C_{36}H_{38}N_{30}O_{40}SiW_{12}Co_2$ (3947.03): C, 11.15; H, 0.83; N, 10.83; Si, 0.72, Found: C, 11.20; H, 0.88; N, 10.61; Si, 0.80. The CCDC number: 1977766.

The synthetic procedure was similar to **$Co^{II/III}_2$-SiW_{12}**, except that the $CoCl_2\cdot 6H_2O$ was used instead of $FeCl_3\cdot 6H_2O$ (160 mg, 0.592 mmol), $ZnCl_2$ (160 mg, 1.173 mmol) and , $CdCl_2\cdot H_2O$ (160 mg, 0.700 mmol). The orange block crystals (Fig. S1) of **$Fe^{II/III}_2$-SiW_{12}** were isolated, washed with distilled water, and dried at room temperature (57% yield based on W). Elemental analyses Calcd for $C_{36}H_{38}Fe_2N_{30}O_{44}SiW_{12}$ (3940.85): C, 10.99; H, 0.82; N, 10.68; Si, 0.71. Found: C, 10.92; H, 0.89; N, 10.56; Si, 0.83. The CCDC number: 1977770. The colorless fusiformis crystals of **Zn^{II}_2-SiW_{12}** were isolated (Fig. S1), washed with distilled water, and dried at room temperature (55% yield based on W). Elemental analyses Calcd for $C_{36}H_{38}Zn_2N_{30}O_{44}SiW_{12}$ (3959.92): C, 10.94; H, 0.82; N, 10.63; Si, 0.71. Found: C, 10.81; H, 0.75; N, 10.72; Si, 0.79. The CCDC number: 1977771. The colorless block

crystals of **Cd^{II}_2-SiW_{12}** were isolated (Fig. S1), washed with distilled water, and dried at room temperature (55% yield based on W). Elemental analyses Calcd for $C_{36}H_{38}Cd_2N_{30}O_{44}SiW_{12}$ (4053.98): C, 10.85; H, 0.81; N, 10.55; Si, 0.71. Found: C, 10.90; H, 0.90; N, 10.62; Si, 0.79. The CCDC number: 1977772.

III. X-ray Crystallography

Single crystal X-ray diffraction data collections of **$Co^{II/III}_2$-SiW_{12}**, **$Fe^{II/III}_2$-SiW_{12}**, **Zn^{II}_2-SiW_{12}** and **Cd^{II}_2-SiW_{12}** were performed using a Bruker Smart Apex CCD diffractometer with Mo-Ka radiation (λ = 0.71073 Å) at 296 K. Multi-scan absorption corrections were applied. The structure was solved by Direct Methods and refined by full-matrix least-squares on F_2 using the SHELXTL 97 crystallographic software package. Anisotropic displacement parameters were used to refine all non-hydrogen atoms. The organic hydrogen atoms were generated geometrically. All H atoms on C atoms were fixed at the calculated positions. The H atoms on water molecules in title compounds cannot be found from the residual peaks and were directly included in the final molecular formula.

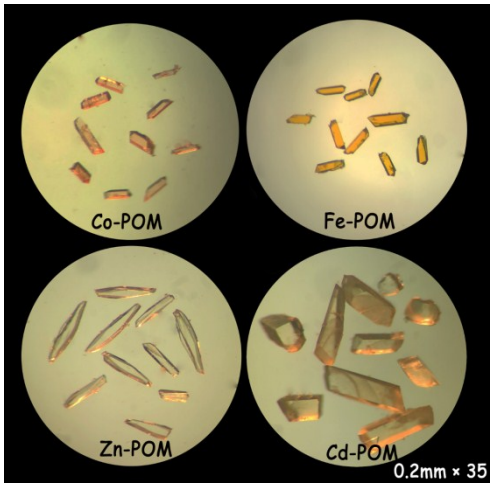

Figure. S1. The images of **$Co^{II/III}_2$-SiW_{12}**, **$Fe^{II/III}_2$-SiW_{12}**, **Zn^{II}_2-SiW_{12}** and **Cd^{II}_2-SiW_{12}** hybrids under an optical microscope (The magnification of optical microscope is 0.25mm × 35).

Table S1 Crystal data and structure refinements for title compounds.

Compound	$Co^{II/III}_2$-SiW_{12}	$Fe^{II/III}_2$-SiW_{12}	Zn^{II}_2-SiW_{12}	Cd^{II}_2-SiW_{12}
Formula	$C_{36}H_{38}Co_2N_{30}O_{44}SiW_{12}$	$C_{36}H_{38}Fe_2N_{30}O_{44}SiW_{12}$	$C_{36}H_{38}Zn_2N_{30}O_{44}SiW_{12}$	$C_{36}H_{38}Cd_2N_{30}O_{44}SiW_{12}$
Formula weight	3947.03	3940.85	3959.92	4053.98
Crystal system	Monoclinic	Monoclinic	Monoclinic	Monoclinic
Space group	C2/c	C2/c	C2/c	C2/c
a/Å	22.301(5)	22.277(5)	22.386(5)	22.237(5)
b/Å	20.140(5)	20.082(5)	19.981(5)	20.176(5)
c/Å	17.499(5)	17.409(5)	17.554(5)	17.670(5)
α/°	90(5)	90(5)	90(5)	90(5)
β/°	107.33(5)	107.03(5)	107.12(5)	106.76(5)
γ/°	90(5)	90(5)	90(5)	90(5)
V/Å^3	7503(3)	7447(3)	7504(3)	7591(3)
Z	4	4	4	4
D_{calcd}/g cm^{-3}	3.487	3.508	3.498	3.540
T/K	293(2)	293(2)	293(2)	293(2)
μ/mm^{-1}	18.871	18.958	19.066	18.776
Refl. Measured	21779	26749	21255	23917
Refl. Unique	6884	9037	6612	9202
R_{int}	0.0653	0.0687	0.0590	0.0293
F(000)	7056	7048	7080	7224
GoF on F^2	1.121	1.001	1.246	1.046
R_1/wR_2 [$I \geq 2\sigma(I)$]	0.0576/0.1188	0.0506/ 0.1053	0.0673/0.1280	0.0534/0.1288

$$R_1 = \sum \| F_o | - | F_c \| / \sum | F_o | \,.\; wR_2 = \sum [w(F_o^2 - F_c^2)^2] / \sum [w(F_o^2)^2]^{1/2}$$

IV. Additional control experiments on photocatalytic hydrogen production of $[M^{II}(pzta)_3]_2$ and $[M^{II}(pzta)_3][M^{III}(pzta)_3]$

Because the **$Co^{II/III}_2$-SiW_{12}** has the best photocatalytic performance among all the title compounds, we have prepared a Co-pzta complex as an example in order to further compare the performance of photocatalytic hydrogen production between **$Co^{II/III}_2$-SiW_{12}** and **Co-pzta** coordination subunit. The **Co-pzta** complex was prepared by an identical synthesis method with the compound **$Co^{II/III}_2$-SiW_{12}**, except that the SiW_{12} POMs had not been added into the reaction system. Consequently, instead of the single crystal, a powder sample with orange color was obtained. The powder sample can be confirmed as a **Co-pzta** complex. The powder contains cobalt cation, which could be confirmed by the orange color, because the single pzta ligand shows

white color (Fig. S16). Meanwhile, the powder contains pzta ligand, which could be confirmed by comparing IR spectra between the obtained powder and the single pzta ligand (Fig. S16). Then, the Co-pzta complex was used as a pholocatalyst to measure the photocatalytic hydrogen production performance by the same experimental conditions as in the manuscript. As shown in Fig. S17, the Co-pzta complex and the parent POM (**SiW_{12}-TBA**) displays a low photocatalytic H_2 production rate. While, the **$Co^{II/III}_2$-SiW_{12}** exhibits superb hydrogen production rates of *ca.* 12245.59 μmol g^{-1} h^{-1}.

V. The details on how to determine the CB positions of Co-pzta coordination subunits and POM

The CB positions of **Co-pzta** complex, **SiW_{12}-TBA** POM and the **$Co^{II/III}_2$-SiW_{12}** photocatalyst are obtained through Mott-Schottky measurement. The typical experiment is listed as follows: before the test, a three-electrode system was constructed. The ITO coated with the photocatalyst was used as the working electrode, platinum wire was used as the counter electrode, Ag/AgCl was used as the reference electrode, and the electrolyte was 0.25M Na_2SO_4 solution. Subsquently, the open circuit voltage was measured, and then the voltage sweep interval was set according to the open circuit voltage. Finally, the IMPE-Impedence-Potential program was used to measure the Mott-schottky curve of the photocatalyst at 1000 Hz. The intersection of the longest linear extension of the curve and the *x*-axis was the flat band potential of the sample.The CB positions of Co-pzta complex and SiW_{12}-TBA POM are shown in Fig. S18.

VI. Discussions on the IR, PXRD and XPS spectra of title compounds.

Herein, we will describe the characterizations of **$Co^{II/III}_2$-SiW_{12}** as an example for concise because the four compounds are isomorphous. The characterizations of The IR spectrurm shows the characteristic bands of an α-Keggin structure at 932, 880, 786 and 675 cm^{-1} (Fig. S5), which can be assigned to to ν(Si-O_c), ν(W=O_t), νas(W-O_b-W) and νas(W-O_c-W),[1] respectively. Additionally, the absorbance peaks at 1638-1163 cm^{-1} belong to organic ligand (pzta). The XRD diffraction peaks of both simulated and experimental patterns match well, which indicates that the phase purity

of the sample is good (Fig. S7). The X-ray photoelectron spectroscopy (XPS) measurements were also done in order to identify the chemical state of the elements and elemental composition of title compounds. The W4f signals fit perfectly to W in the oxidation state +VI. As shown in Fig. S8 and S9, the XPS high-resolution spectrum of the W4f of $\mathbf{Co^{II/III}_2\text{-}SiW_{12}}$ shows two main peaks 34.43 eV and 36.58 eV that are assigned to W $4f_{7/2}$ and W $4f_{5/2}$, respectively.[2] For the Co2p spectrum of $\mathbf{Co^{II/III}_2\text{-}SiW_{12}}$, it is apparent that two main peaks are located at 780.68 eV and 796.84 eV, and meanwhile there are two dithered satellite peaks at 786.69 eV and 802.94 eV (Fig. S8). The peaks of Co $2p_{3/2}$ and Co $2p_{1/2}$ in the Co 2p spectrum can be fitted to two peaks after Gaussian fitting. The fitted peaks of 780.28 eV and 795.50 eV are attributed to Co^{2+}, and the fitted peaks of 781.90 eV and 797.90 eV belong to Co^{3+}.[3] In all, the results of IR, PXRD and XPS characterizations are consist with the analysis of single crystal X-ray diffraction.

VII. Experimental process on photocatalytic hydrogen evolution

All photocatalytic experiments were conducted in a 27 mL Pyrex reaction vessel via a photocatalytic H_2 evolution activity evaluation system, where the photoreaction temperature was kept at a constant temperature (4 °C) with circulating water through a thermostat. The gas circulation was swept by high purity N_2 before illumination. For each experiment, the 5 mg photocatalyst was dispersed in 20 mL of 10 vol % triethylamine (TEA) and 50 vol% acetone aqueous solution under a 500 W Xe lamp (without cut-off filter). Place the reactor on a stirrer and continue to stir and irradiate for 3h, enabling the photocatalyst to maintain a uniform dispersion state and uniform illumination during the experimental process. The amount of hydrogen evolved was determined at an interval of 1 h with gas chromatography.

Section 2 Supplementary structural figures and characterization information

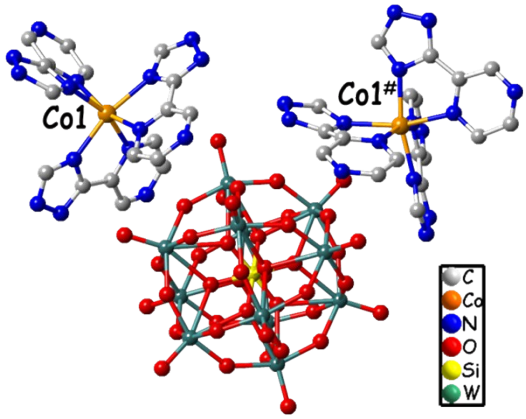

Figure S2. View of the basic crystallographic unit in $\mathbf{Co^{II/III}_2\text{-}SiW_{12}}$ (All H atoms and lattice water molecules are omitted for clarity). (Symmetry code: # = 2-x, y, 0.5-z).

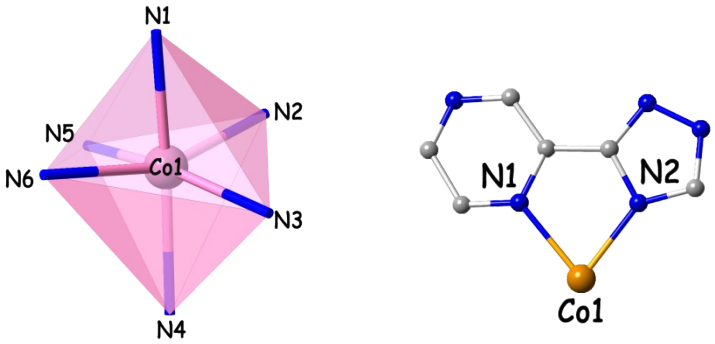

Figure S3. The coordination modes of crystallographically independent Co cation and pata ligand in $\mathbf{Co^{II/III}_2\text{-}SiW_{12}}$.

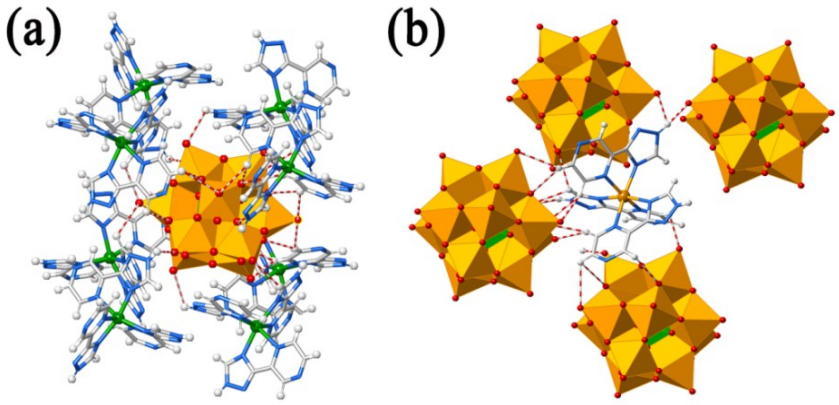

Figure S4. Ball and stick views of the coordination environments of (a) SiW_{12} cluster; (b) $\{Co(pzta)_3\}$ fragment in $\mathbf{Co^{II/III}_2\text{-}SiW_{12}}$.

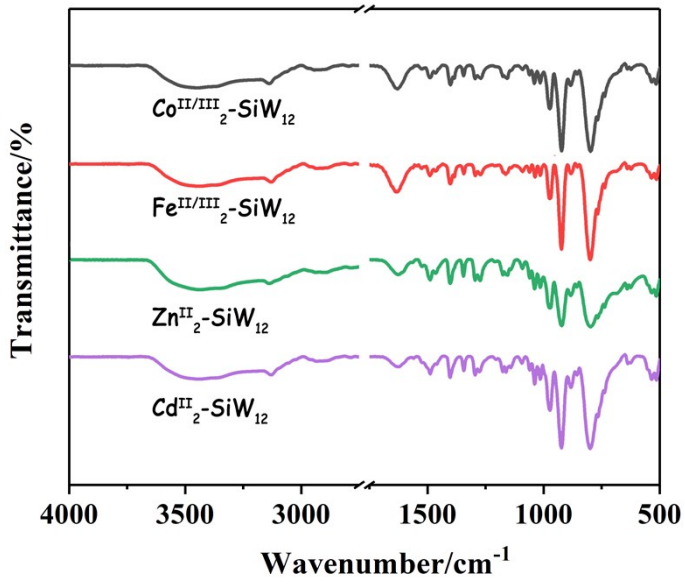

Fig. S5. The IR spectra of **Co$^{II/III}_2$-SiW$_{12}$**, **Fe$^{II/III}_2$-SiW$_{12}$**, **Zn$^{II}_2$-SiW$_{12}$** and **Cd$^{II}_2$-SiW$_{12}$**.

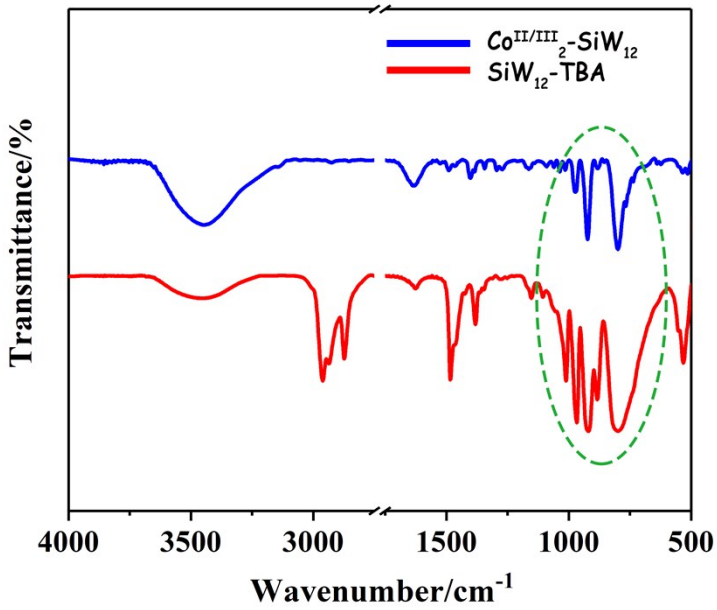

Fig. S6. The IR spectra of **Co$^{II/III}_2$-SiW$_{12}$** and **SiW$_{12}$-TBA**, .

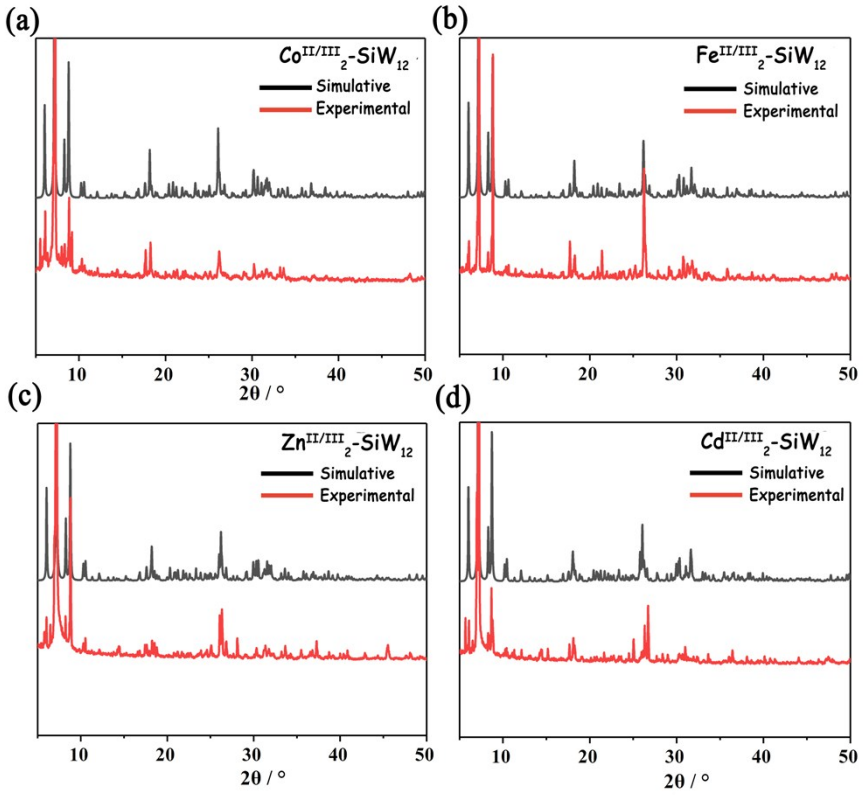

Fig. S7. Stimulative (black) and experimental (red) PXRD patterns for **Co$^{II/III}_2$-SiW$_{12}$**, **Fe$^{II/III}_2$-SiW$_{12}$**, **Zn$^{II}_2$-SiW$_{12}$** and **Cd$^{II}_2$-SiW$_{12}$**.

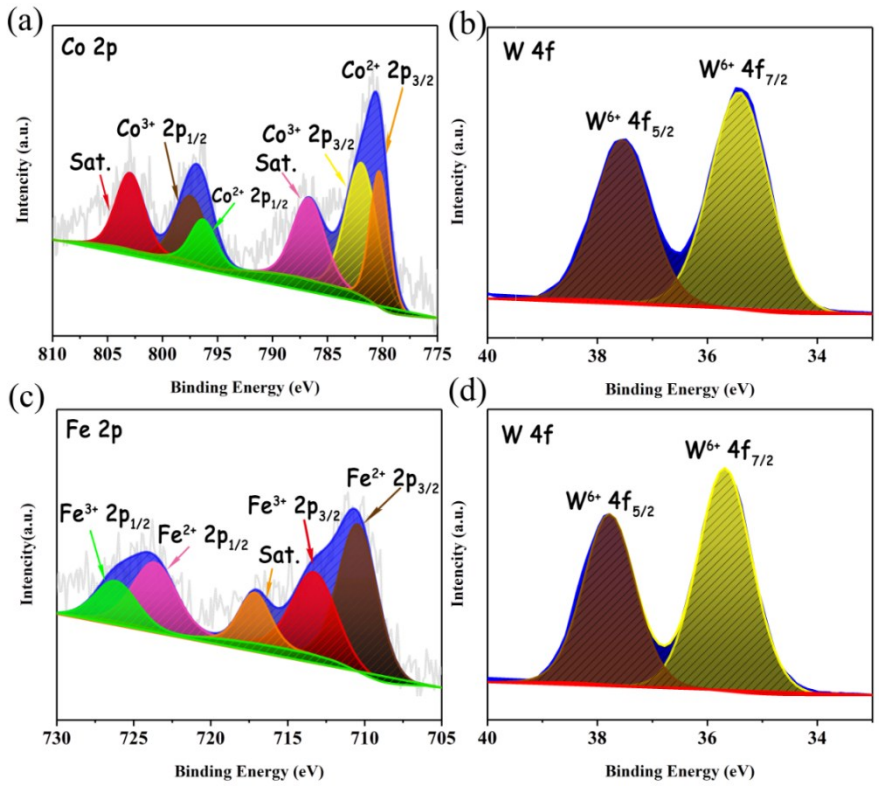

Fig. S8. (a-b) Co 2p and W 4f XPS spectra of **Co$^{II/III}_2$-SiW$_{12}$**, (c-d) Fe 2p and W 4f XPS spectra of **Fe$^{II/III}_2$-SiW$_{12}$**.

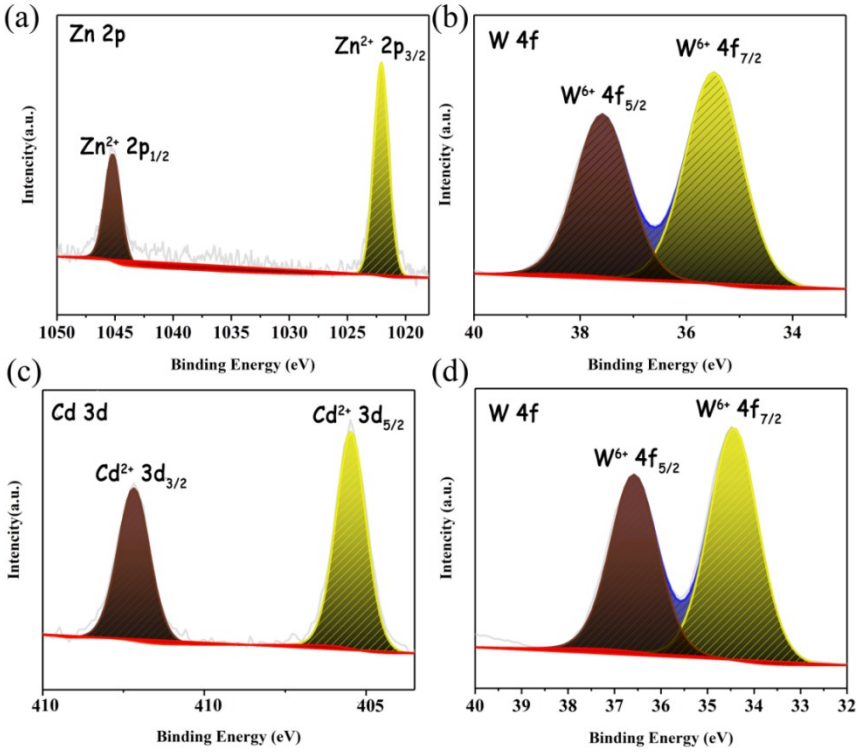

Fig. S9. (a-b) Zn 2p and W 4f XPS spectra of $\mathbf{Zn^{II}_2\text{-}SiW_{12}}$, (c-d) Cd 3d and W 4f XPS spectra of $\mathbf{Cd^{II}_2\text{-}SiW_{12}}$.

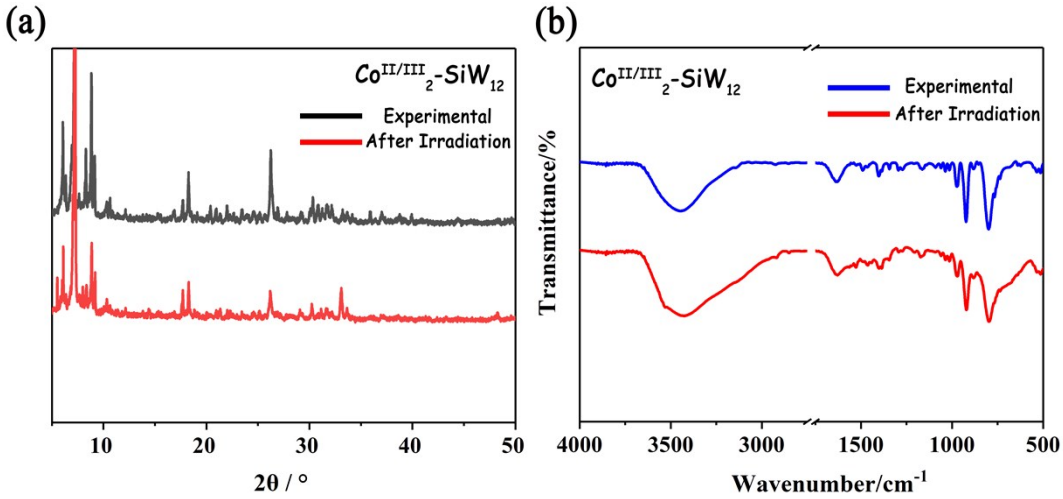

Fig. S10. (a) $\mathbf{Co^{II/III}_2\text{-}SiW_{12}}$ PXRD patterns of the experimental synthesis (black), and the catalyst after reactions (red); (b) The IR spectrum of $\mathbf{Co^{II/III}_2\text{-}SiW_{12}}$ before and after reactions.

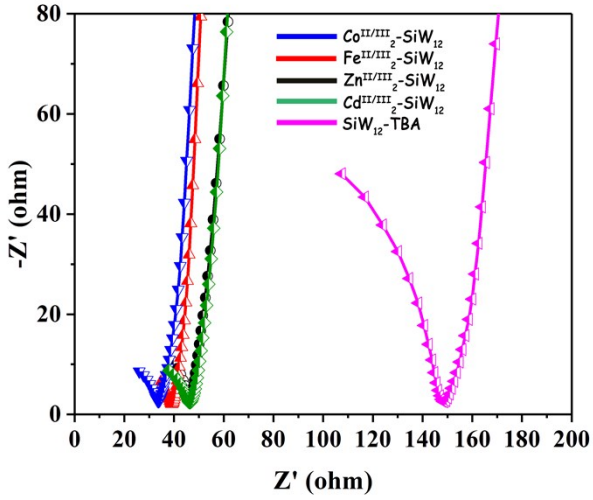

Fig. S11. EIS Nyquist plots of title compounds.

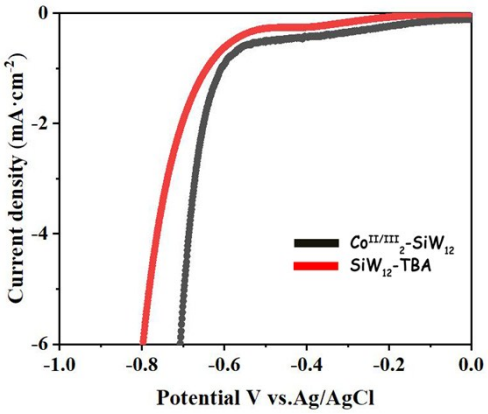

Fig. S12. Liner sweep voltammetry (LSV) curves of **Co$^{II/III}_2$-SiW$_{12}$** and **SiW$_{12}$-TBA**.

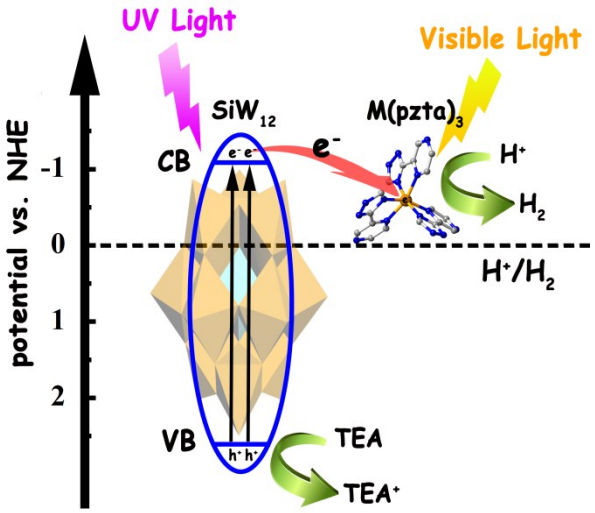

Fig. S13. The proposed mechanism of the photocatalytic reaction.

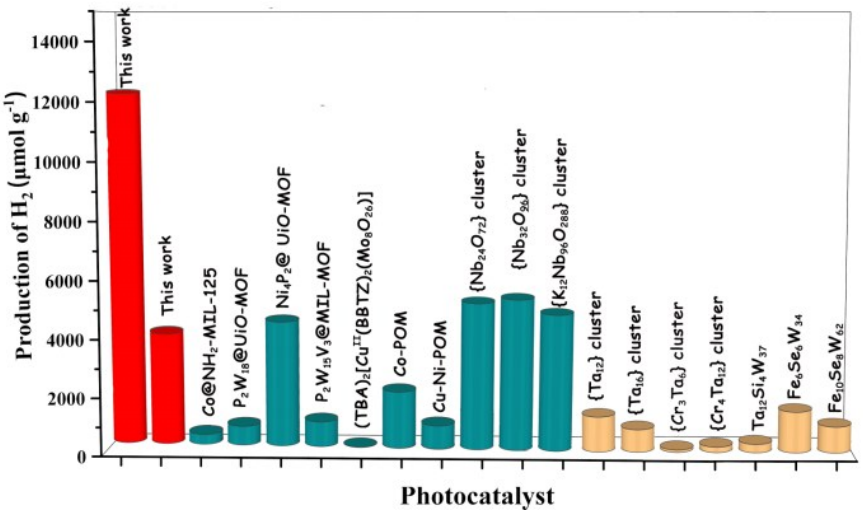

Fig. S14. Comparison of POM-photocatalysts on H_2 production.

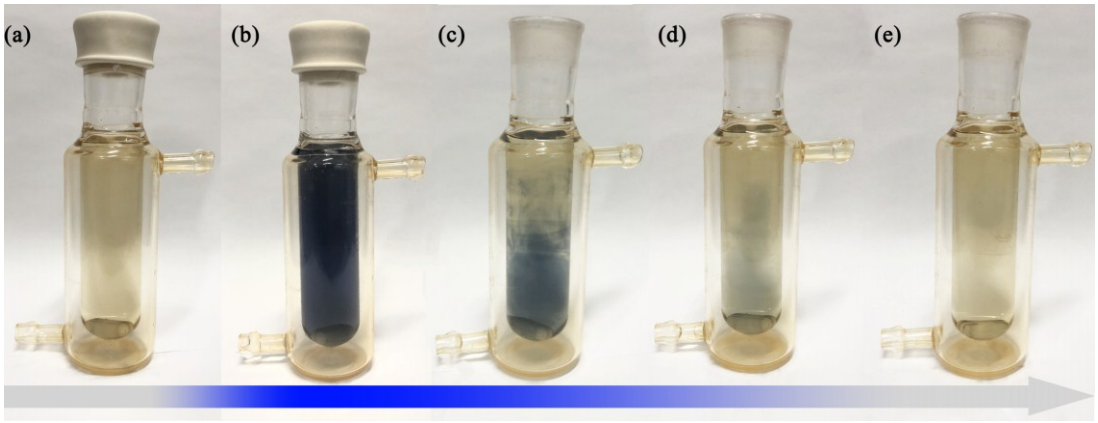

Fig. S15. Optical image: (a) $\mathbf{Co^{II/III}_2\text{-}SiW_{12}}$ photocatalytic system solution before irradiation. (b) heterpolyblue (HPB) of $\mathbf{Co^{II/III}_2\text{-}SiW_{12}}$ photocatalytic system solution after irradiation. (c-e) HPB turn to HPA of $\mathbf{Co^{II/III}_2\text{-}SiW_{12}}$ photocatalytic system solution after expose O_2.

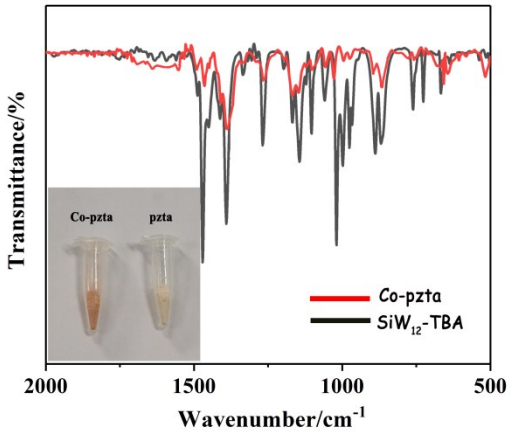

Fig. S16. IR spectra of the pzta ligand and Co-pzta compound. (inset: optics images of corresponding pzta ligand and Co-pzta); (right)

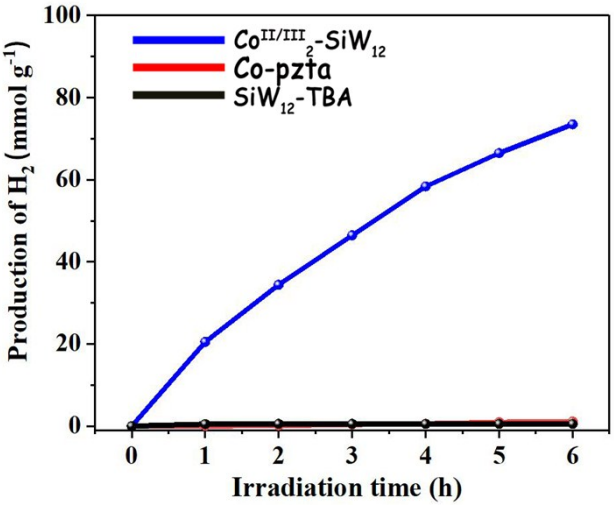

Fig. S17. The photocatalytic H_2 evolution activities of **$Co^{II/III}_2$-SiW_{12}**, **Co-pzta** and **SiW_{12}-TBA**.

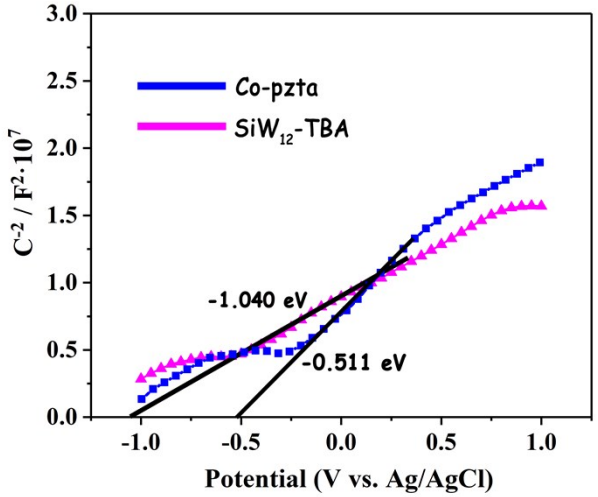

Fig. S18. Mott-Schottky plots of **Co-pzta** complex and **SiW_{12}-TBA**.

Section 3 Some detailed comparisons and summaries

Table S2. Summary of parallel experiments and optimum experimental conditions

Catalyst	Amount (mg)	Light (λ/nm)	Electron donor	H_2 production (μmol g^{-1} h^{-1})
$Co^{II/III}_2$-SiW_{12}	5	＞190	TEA (2ml)	12245.59
$Co^{II/III}_2$-SiW_{12}	5	＞190	TEA (4ml)	4723.57
$Co^{II/III}_2$-SiW_{12}	5	＞190	TEA (no acetone)	trace
$Co^{II/III}_2$-SiW_{12}	5	＞190	TEOA (2ml)	187.12
$Co^{II/III}_2$-SiW_{12}	5	＞190	CH_3OH (5ml)	184.47
$Co^{II/III}_2$-SiW_{12}	5	＞190	Lactic Acid (5ml)	trace
$Co^{II/III}_2$-SiW_{12}	5	＞190	L-Ascorbic Acid Sodium Salt (0.05g)	trace
Co-pzta	5	＞190	TEA (2ml)	178.49
$Co^{II/III}_2$-SiW_{12}	5	>400	TEA (2ml)	no
$Co^{II/III}_2$-SiW_{12}	5	<400	TEA (2ml)	trace
$Fe^{II/III}_2$-SiW_{12}	5	＞190	TEA (2ml)	3912.78
Zn^{II}_2-SiW_{12}	5	＞190	TEA (2ml)	121.45
Cd^{II}_2-SiW_{12}	5	＞190	TEA (2ml)	112.91
SiW_{12}-TBA	5	＞190	TEA (2ml)	86.31
SiW_{12}-TBA	5	>400	TEA (2ml)	no
SiW_{12}-TBA	5	<400	TEA (2ml)	trace
No catalyst	-	＞190	TEA (2ml)	no
No light	5	-	TEA (2ml)	no
No donor	5	＞190	-	no

Table S3. Summary of H_2 evolution activity of typical photocatalysts: I typical POM-based metal-organic photocatalysts (green background); II typical POMs and noble metals composite photocatalysts (orange background); III Other typical excellent photocatalysts (blue background); IV the photocatalysts reported by this work (red background).

Catalyst	Co-catalyst	SED	Illumination (nm)	Activity, ($\mu molg^{-1}h^{-1}$)	Ref
I typical POM-based metal-organic photocatalysts					
Co@NH_2-MIL-125(Ti)[4]	$Co^{III}Br_2LH$	TEA	λ>408	350	*Energ. Environ. Sci.*, 2015, 8, 364-375
P_2W_{18}@UiO-MOF[5]	POM	Methanol	λ>400	669	*J. Am. Chem. Soc.*, 2015, 137, 9, 3197-3200
Ni_4P_2@ UiO-MOF[6]	POM	Methanol	λ>400	4400	*Angew. Chem. Int.*, 2016, 23, 6411-6416
$P_2W_{15}V_3$ @MIL-MOF[7]	POM	TEOA	λ>400	883	*Appl. Catal. B-Environ.*, 2018, 224, 46-52
$(TBA)_2[Cu^{II}(BBTZ)_2(Mo_8O_{26})]$[8]	Pt	Methanol	λ＜400	7.8	*Angew. Chem. Int.*, 2012, 6, 7985-7989
Co-POM[9]	Co	TEA	λ＞380	2000	*ACS Appl. Mater. Interfaces.*, 2018, 10, 13462-13469.
Cu-Ni-POM[10]	Cu/Ni	TEA	λ＞380	824	*Chem. Commun.*, 2019, 55, 3805-3808
$\{Nb_{24}O_{72}\}$ Cluster[11]	$Co^{III}(dmgH)_2$ pyCl	TEA	λ=365	5161.4	*J. Am. Chem. Soc.* 2012, 134, 14004−14010.
$\{Nb_{32}O_{96}\}$ cluster[11]	$Co^{III}(dmgH)_2$ pyCl	TEA	λ=365	5312.5	*J. Am. Chem. Soc.* 2012, 134, 14004−14010.
$\{K_{12}Nb_{96}O_{288}\}$ cluster[11]	$Co^{III}(dmgH)_2$ pyCl	TEA	λ=365	4804.1	*J. Am. Chem. Soc.* 2012, 134, 14004−14010.
II typical POMs and noble metals composite photocatalysts					
$\{Ta_{12}\}$ cluster[12]	Pt	CH_3OH	λ=365	1250	*J. Am. Chem. Soc.* 2012, 134, 19716−19721.
$\{Ta_{16}\}$ cluster[12]	Pt	CH_3OH	λ=365	803	*J. Am. Chem. Soc.* 2012, 134, 19716−19721.
$\{Cr_3Ta_6\}$ cluster[13]	Pt	CH_3OH	500 Xe	89.2	*J. Mater. Chem. A*, 2017,5, 22970-22974.
$\{Cr_4Ta_{12}\}$ cluster[13]	Pt	CH_3OH	500 Xe	198.30	*J. Mater. Chem. A*, 2017,5, 22970-22974.
$\{Ta_{12}Si_4W_{37}\}$[14]	Pt	CH_3OH	500 Xe lamp	301.2	*Dalton Trans., 2017,46, 10177-10180*
$\{Fe_6Se_6W_{34}\}$[15]	Fe^{III}	CH_3OH	500 Hg lamp	1447.5	*Chem. Commun., 2014,50, 13265-13267.*
$\{Fe_{10}Se_8W_{62}\}$[15]	Fe^{III}	CH_3OH	500 Hg	925.0	*Chem. Commun., 2014,50, 13265-*

			lamp		*13267.*
III Other typical excellent photocatalysts					
TFPT-COF[16]	Pt	TEOA	λ>420	1970	*Nat. Commun.*, 2015, 6, 8508.
g-C_3N_4 nanosheets[17]	Pt	TEOA	λ>420	1860	*Adv. Mater.*, 2013, 25, 2452-2456.
g-C_3N_4[18]	MoS_2	Lactic acid	λ>420	1030	*Angew. Chem. Int. Ed*, 2013, 52, 3621-3625.
MOF-5[19]	Ni	TEOA	λ> 420	3022	*Appl. Catal. B-Environ.*, 2016, 190, 12-25.
Au@CdS/MIL-101[20]	Au	Na_2S and Na_2SO_3	λ>420	2500	*Appl. Catal. B-Environ.*, 2016, 185, 307-314.
IV the photocatalysts reported by this work					
$Co^{II/III}_2$-SiW_{12}	**$Co(pzta)_3$**	**TEA**	**λ＞190**	**12245.59**	**This work**
$Fe^{II/III}_2$-SiW_{12}	**$Fe(pzta)_3$**	**TEA**	**λ＞190**	**3912.78**	**This work**

References

1 D. F. Chai, Y. Hou, K. P. O'Halloran, H .J. Pang, H .Y. Ma, G. N. Wang, X. M.Wang, *ChemElectroChem,* 2018, **5**, 3443-3450.

2 D. F. Chai, C.J. Gómez-García, B. N. Li, H .J. Pang, H .Y. Ma, Chem. Eng. J., 2019, **373**, 587-597.

3 J. H. Zheng, L. Zhang, Appl. Catal. B-Environ., 2018, **237**, 1-8.

4 M. A. Nasalevich, R. Becker, E. V. Ramos-Fernandez, S. Castellanos, S. L. Veber, M. V. Fedin, F. Kapteijn, J. N. H. Reek, J. I. van der Vlugt and J. Gascon, Energy Environ. Sci., 2015, **8**, 364-375.

5 Z. M. Zhang, T. Zhang, C. Wang, Z. K. Lin, L. S. Long, and W. B. Lin, J. Am. Chem. Soc. 2015, 137, **9**, 3197-3200.

6 J. K. Xiang, Z. K. Lin, Z. M. Zhang, T. Zhang, W. B. Lin, Angew. Chem. Int., 2016, **23**, 6411-6416.

7 H. Li, S. Yao, H. L. Wu, J. Y. Qu, Z. M. Zhang, T. B. Lu, W. B. Lin, E. B. Wang, Appl. Catal. B-Environ., 2018, **224**, 46-52.

8 H. Fu, C. Qin, Y. Lu, Z. M. Zhang, Y. G. Li, Z. M. Su, W. L. Li, E. B. Wang, Angew. Chem. Int., 2012, **6**, 7985-7989

9 W. L. Sun, B. W. An, B. Qi, T. Liu, M. Jin, and C.Y. Duan, ACS Appl. Mater. Interfaces., 2018, **10**, 13462-13469.

10 W. L. Sun, C. He, T. Liu and C.Y. Duan, Chem. Commun., 2019, **55**, 3805-3808.

11 P. Huang, C. Qin, Z.M. Su, Y. Xing, X.L. Wang, K.Z. Shao, Y.Q. Lan, E. B. Wang, J. Am. Chem. Soc. 2012, **134**, 14004−14010.

12 S. J. Li, S. M. Liu, S. X. Liu, Y. W. Liu and J. H. Ye, J. Am. Chem. Soc., 2012, **134**, 19716-19721.

13 P. Huang, X. J. Wang, J. J. Qi, X. L. Wang, M. Huang, H. Y. Wu, C. Qin and Z. M. Su, J. Mater. Chem. A, 2017, **5**, 22970-22974.

14 P. Huang, H. Y. Wu, M. Huang, M. Du,C. Qin, X. L. Wang, and Z. M. Su, Dalton Trans., 2017,**46**, 10177-10180.

15 W. C. Chen, C. Qin, X. L. Wang, Y. G. Li, H. Y. Zang, Y. Q. Jiao, P. Huang, K. Z. Shao, Z. M. Su and E.B. Wang, Chem. Commun., 2014,**50**, 13265-13267.

16 V. S. Vyas, F. Haase, L. Stegbauer, G. Savasci, F. Podjaski, C. Ochsenfeld and B. V. Lotsch, Nat. Commun., 2015, **6**, 8508.

17 S. Yang, Y. Gong, J. Zhang, L. Zhan, L. Ma, Z. Fang, R. Vajtai, X. Wang and P. M. Ajayan, Adv. Mater., 2013, **25**, 2452-2456.

18 Y. Hou, A. B. Laursen, J. Zhang, G. Zhang, Y. Zhu, X. Wang, S. Dahl and I. Chorkendorff, Angew. Chem. Int. Ed, 2013, **52**, 3621-3625.

19 W. L. Zhen, J. T. Ma, G. X. Lu, Appl. Catal B., 2016, **190**, 12-25.

20 Y. J. Wang, Y. N. Zhang, Z. Q. Jiang, G. Y. Jiang, Z. Zhao, Q. H. Wu, Y. Liu, Q. Xu, A. J. Duan, C. M. Xu, Appl. Catal B., 2016, **185**, 307-314.